Design and Experimental Demonstration of a YBCO Toroidal Magnet

L. Ren, H. Liu, X. Deng, Y. Liao, Y. Xu, J. Li, J. Shi, Y. Tang, P. Han, H. Liu, and J. Chen

***Abstract*—A laboratory-scale toroidal magnet was designed and tested in this paper to explore the feasibility of YBCO tapes applied to tokamak technology. The magnet consists of 12 D-shaped double-pancake subcoils arranged in the circumference of 80 mm; the outer radius is 280 mm. The magnet is conduction-cooled by two cryocoolers. We conducted a series of experiments on the prototype to investigate the properties of the magnet at 20 K, and the results show that the maximum current capacity is 200 A and the storage energy is 6.4 kJ.**

***Index Terms*—Conduction cooling, HTS magnet, tokamak, toroidal magnet, YBCO.**

I. Introduction

A tokamak has three main magnet systems: the toroidal field (TF) magnet, poloidal field (PF) magnet and central solenoid (CS) magnet. The TF magnet creates a primary confining toroidal field, while the PF magnet is used for shaping, stability, and position control of the confined plasma. Both the PF and TF magnets must carry large current for significant durations, especially in long-pulse or steady-state tokamaks [1]. Thus, it is essential to use superconducting coils for future fusion power generation devices, so as to reduce tokamak magnet energy consumption and ensure the system's security and stability.

As of now, only low temperature superconducting (LTS) conductors such as NbTi and Nb_3Sn [2] have been applied to tokamak magnets (except current leads). Compared to LTS magnets, high temperature superconducting (HTS) magnets have lower cooling cost [3]—and further, for YBCO tapes, show attractive cost-saving potential. As such, HTS conductors are a promising possible application for tokamak magnets [4].

In ITER, BSCCO conductors have been used for current leads and bus bars. Certain inherent problems such as lack of high current conductor and coil development, and the high-cost obstacle remain unresolved, so HTS conductors have not been introduced into tokamak magnets on any large scale. At present, YBCO commercial products are available and show mechanical and electromagnetic properties better than BSCCO [6], [7]. In the near future, it may be possible to apply them successfully to tokamak magnets provided single YBCO tape can be made long enough to meet the requirements for winding tokamak coils and YBCO cables can be manufactured.

In this study, as a first step toward feasibly realizing YBCO tapes for tokamak magnets, we designed and tested a laboratory-scale YBCO toroidal magnet.

①DCQPS; ②Power source; ③HTS magnet; ④Oscilloscope; ⑤CS

Fig. 1. Overview of the YBCO toroidal magnet system.

II. Magnet System

The YBCO toroidal magnet system consists of three parts, the HTS magnet, data collection and quench protection system (DCQPS), and cryogenic system (CS), as shown in Fig. 1.

A. YBCO Tape and Magnet

The magnet consists of 12 D-shaped, double-pancake YBCO coils. The coils are made of Amperium 8501 YBCO tape (4.8 mm width $\times$ 0.2 mm thickness, with minimum nominal current 90 A at 77 K and self-field) from AMSC. The 12 coils were evenly distributed in a circle plate with inner and outer diameters of 100 mm and 800 mm, respectively. The magnet's structure is shown in Fig. 2 and its parameters are listed in Table I.

B. Cryogenic System

We set the operating temperature of the magnet to 20 K. The magnet was cooled with a single-stage GM cryocooler

Manuscript received September 4, 2015; accepted March 2, 2016. Date of publication March 4, 2016; date of current version March 18, 2016. This work was supported in part by the Specialized Research Fund for ITER under Grant 2011GB113004 and in part by the Fundamental Research Funds for the Central Universities, HUST, under Grant 2014TS145.

L. Ren, H. Liu, X. Deng, Y. Liao, Y. Xu, J. Li, J. Shi, and Y. Tang are with the State Key Laboratory of Advanced Electromagnetic Engineering and Technology, Huazhong University of Science and Technology, Wuhan 430074, China (e-mail: renli@mail.hust.edu.cn).

P. Han, H. Liu, and J. Chen are with the Institute of Plasma Physics, Chinese Academy of Sciences, Hefei 230031, China.

Color versions of one or more of the figures in this paper are available online at http://ieeexplore.ieee.org.

Digital Object Identifier 10.1109/TASC.2016.2538459

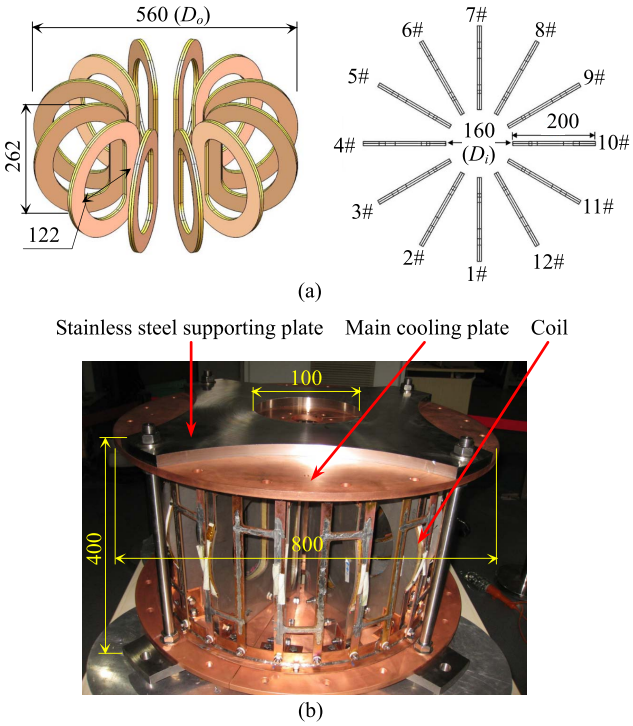

Fig. 2. YBCO toroidal magnet. (a) Layout of 12 D-shaped coils. (b) The magnet.

TABLE I
MAGNET PARAMETERS

Designation	Parameter
Maximal outer magnet diameter	800 mm
Minimal inner magnet diameter	100 mm
Total height of magnet	400 mm
Width of D-shaped coil	200 mm
Number of turns of every coil	228
Number of joints	11
Total length of tape	1800 m
Operating temperature T	20 K
Maximal current capacity I	200 A
Inductance L	0.41 H

1# (Type AL330, 40 W @ 20 K, Cryomech Inc., USA) while the radiating shield and the hybrid current leads were cooled by a two-stage GM cryocooler 2# (Type KDE415-KDC6000, 6 W @ 20 K, 110 W @ 77 K, Nanjing Kede Cryogenic Technology Co., LTD, China). Each coil was connected with two main conduction cooling plates at both ends of the magnet through two 1 mm-thick OFHC copper plates. Fig. 3 shows the conduction cooling structure and positions of sensors on the magnet.

C. Data Collection and Quench Protection System (DCQPS)

The DCQPS is comprised of three parts: Keithley3706 data acquisition instrument, industrial computer, and quench protection subsystem. Based on LabVIEW, data were collected with the Keithley3706 instrument and sent to an industrial computer to be processed, saved and displayed during the experiment. The collected data include each coil's voltage, the main section temperatures of the magnet and conduction cooling system, and magnetic flux densities between the two coils (M1) and inside the center of one of the coils (M2 or M3). The position of sensors is shown in Fig. 3.

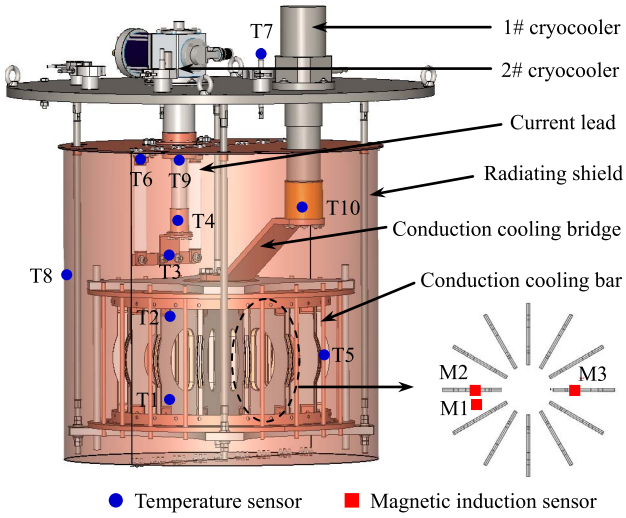

Fig. 3. Conduction-cooling structure and position of sensors.

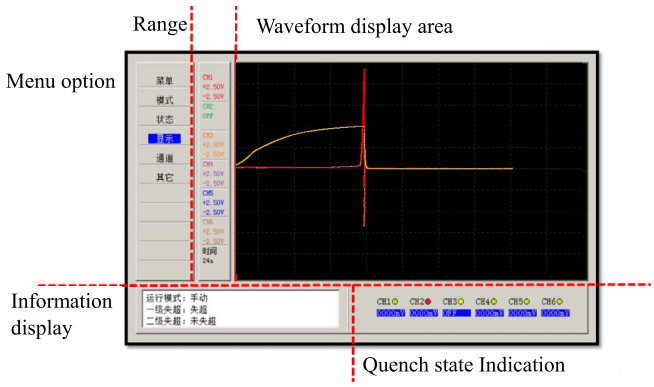

Fig. 4. Human–machine interactive interface.

We used the same quench detection method and protection strategy as those in a previously published study [8]. The subsystem also has a human-machine interactive interface, where we can set the threshold value of the quench voltage and manage the running state of the magnet (shown in Fig. 4).

III. MAGNET DESIGN

A. D-Shaped Coil Configuration

The D-shaped coil is one unit coil of the YBCO toroidal magnet, first proposed by J. File [9] to provide necessary mechanical support against the massive electromagnetic force in a tokamak nuclear fusion reactor. The D-shaped curve's

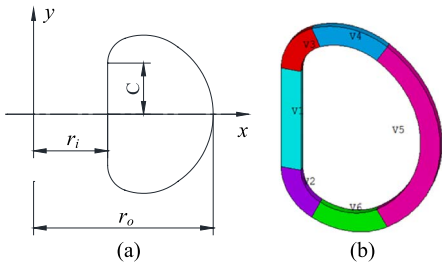

Fig. 5. D-shaped curve and six-section model. (a) Sketch of the D-shaped curve. (b) Six-section model of the D-shaped coil.

mathematical characteristic can be expressed as Eq. (1), and its curve sketch is as shown in Fig. 5(a)

$$y = \pm \int_{r_i}^{r_o} \left(\frac{\ln x}{\sqrt{k^2 - \ln^2 x}} \right) dx \mp C, \; x \in [r_i, r_o]$$
$$k = \ln \sqrt{\left(\frac{r_o}{r_i} \right)} \tag{1}$$

where C is a constant that determines the up-and-down position of the D-shaped curve along the y axis, while r_i and r_o are the inner and outer radii, respectively.

In our design, the D-shaped curve was simplified as a combination of five arc segments and one linear segment vertical symmetrical in the simulated modeling, as shown in Fig. 5(b). Owing to that the size of the magnet is relatively small, the electromagnetic calculation error caused by the simplification process can be ignored.

B. Design Goal and Method

Our design objectives and restrictions were stated as follows: the maximal operating current was 200 A @ 20 K, energy storage capacity was above 5 kJ with fixed usage of 2 km YBCO tapes, the parallel magnetic field was as high as possible, and the unit coil was a D-shaped double pancake wound with a single length of tape without splices. The number of coils (N), inner diameter (D_i) and the outer diameter (D_o) of the magnet served as design variables, while parameters such as the coil thickness and the number of coil turns were dependent variables.

We used finite element method (FEM) analysis combined with MATLAB to design the prototype. A flowchart of the calculation procedure is shown in Fig. 6.

We used MATLAB to control and call the FEM program for electromagnetic calculation, then used the calculation results for post-processing. Finally, we obtained the optimal scheme at $N = 12$, $D_i = 160$ mm and $D_o = 560$ mm (see Fig. 2(a)). The maximal operating current and energy storage capacity were 200 A and 5.6 kJ, respectively, and the inductance L was 0.28 H. Then, the dimensions of the D-shaped coil were then determined and shown in Fig. 7(a), and the wound D-shaped, double-pancake coil is shown in Fig. 7(b).

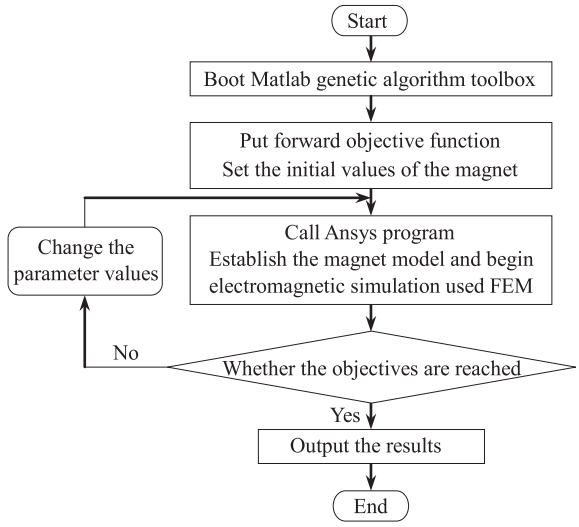

Fig. 6. Electromagnetic design flowchart.

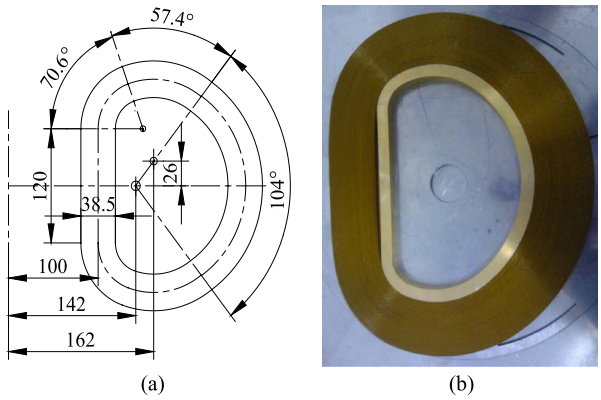

Fig. 7. D-shaped coil. (a) Dimensions of the coil. (b) The wound coil.

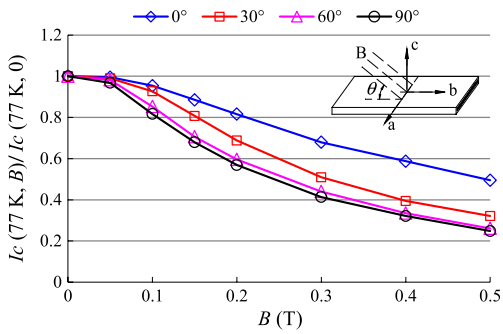

Fig. 8. Normalized current of tape dependent on field and angle at 77 K.

C. Critical Current Evaluation

The expected maximal operating current of the magnet was estimated as the crossing point of the load line of the magnet and the critical current characteristic curve of the YBCO tape. Fig. 8 shows the experimentally obtained normalized current curve of the Amperium TM8501 YBCO tape, as dependent on magnetic field angle θ at 77 K.

As shown in Fig. 8, critical current degradation was greater in the normal magnetic field (relative to the tape surface),

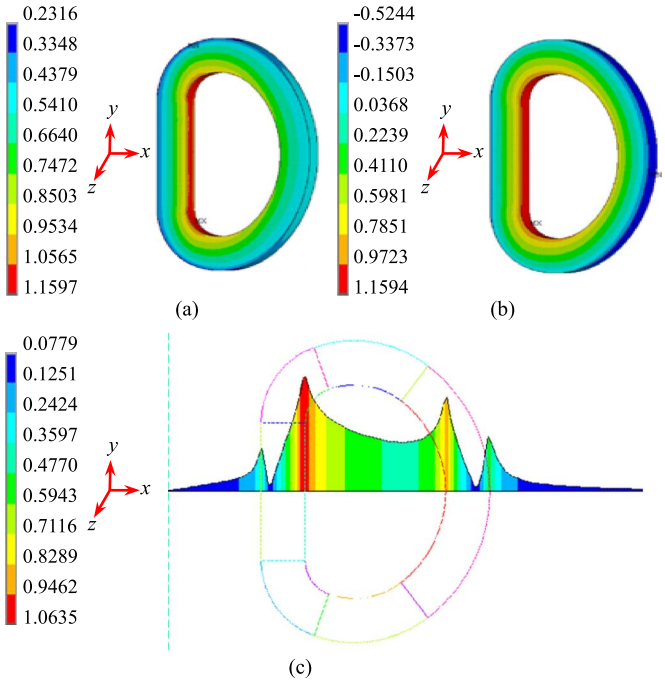

Fig. 9. Magnetic field distribution of the magnet, where $I = 200$ A at 20 K. (a) Magnetic field amplitude. (b) Magnetic field parallel to the z-axis. (c) Magnetic field along the radial distance x.

especially in the perpendicular field $(\theta = 90°, B \perp c)$ as opposed to the parallel field $(\theta = 0, B//c)$. Further, the current degradation grew more severe as magnetic field B increased.

Fig. 9 shows the magnetic field distribution of the YBCO toroidal magnet fed with the current of 200 A at 20 K. The magnetic field along the radial distance (x-axis direction) was unevenly distributed, and the leakage magnetic field dropped quickly to zero when the distance from the origin exceeded the outer radius; in effect, the magnet produced a quite small leakage magnetic field. In addition, the linear segment of the magnet bore the largest parallel field component (the largest magnetic field parallel to the tape surface or z-axis, 1.1594 T) which was close to the highest magnetic field amplitude (1.1597 T), while the upper and lower arc segments near to the linear segment bore the largest perpendicular field component (the largest magnetic field perpendicular to the tape surface, 0.6044 T). Consequently, the maximal operating current of the magnet is determined by one of the two applied on these sections.

Fig. 10 shows the $I_c - B$ characteristic of the YBCO tape at 20 K, the magnet load line $I_{//B}$ under the parallel field component, and the magnet load line $I_{\perp B}$ under the perpendicular field component.

As shown in Fig. 10, we obtained two typical operating current values: 301 A corresponding to the crossing point (1.75 T, 3.345) and 200 A corresponding to the crossing point (0.6 T, 2.22). The smaller one (200 A) limits the performance of the magnet, thus it represents the maximal expected operating current of the system.

IV. Experimental Tests

A series of experiments were conducted to verify the performance of the proposed magnet system including cool-down characteristic, inductance characteristic dependent on frequency, and current-carrying characteristic. The experimental circuit is shown in Fig. 11.

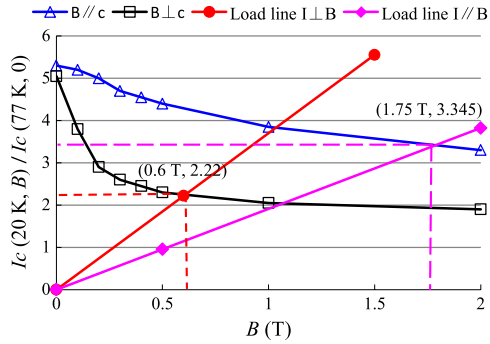

Fig. 10. $I_c - B$ curve of YBCO tape and the magnet load line at 20 K.

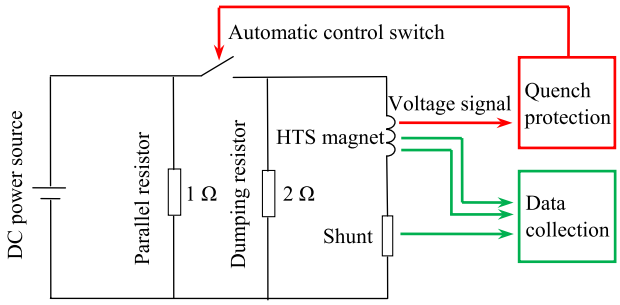

Fig. 11. Experimental circuit.

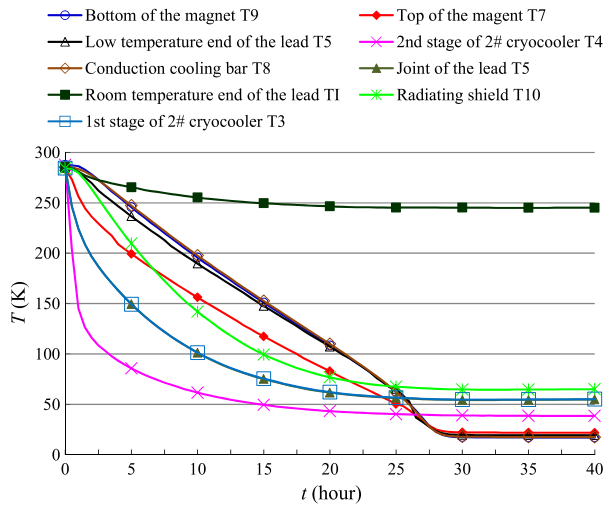

Fig. 12. Temperature variation during cooldown.

The DC power source (PSI 8080-340 3U, Elektro-Automatik, Germany) was protected by a 1 Ω parallel resistor during the experiment, and a 2 Ω dumping resistor protected the HTS magnet.

A. Cool-Down Characteristic

Fig. 12 shows the temperature variation characteristics of the YBCO toroidal magnet during the cool-down process.

TABLE II
MAGNET TEMPERATURES DURING OPERATION

Position	Temperature
Bottom of the magnet (T1)	17.6 K
Top of the magnet (T2)	18.1 K
Low temperature end of the current lead (T3)	19.4 K
Second stage of 2# cryocooler (T4)	38.5 K
Conduction cooling bar (T5)	17.6 K
Joint of the current lead (T6)	54.8 K
Room-temperature end of the current lead (T7)	245.1 K
Radiating shield (T8)	65.1 K
First stage of 2# cryocooler (T9)	54.1 K
Cold head of 1# cryocooler (T10)	16.5 K

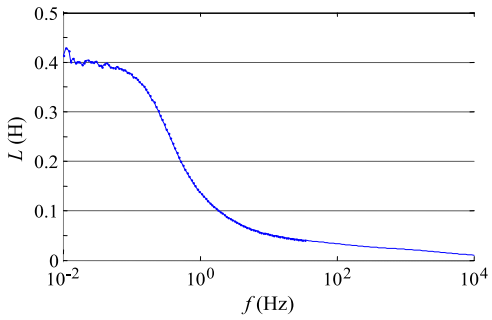

Fig. 13. Inductance L dependent on frequency f.

It took about 30 hours for the magnet to reach the rated operating temperature (20 K) and about 40 hours for the magnet system to reach thermal balance. After that, the magnet maintained stable temperature levels throughout the experiment as shown in Table II.

The temperature at both ends of the magnet (T1 and T2) and the one at the current leads (T3) fell between 17.6 K and 19.4 K, i.e., were lower than the design value of 20 K (Table II). The temperatures at the other parts of the magnet also met operating requirements.

B. Inductance Characteristic Dependent on Frequency

In general, the inductance L of a magnet is closely related to its energy storage, so we used a LCR tester to measure the inductance L dependent of frequency f in the prototype. The test results are indicated in Fig. 13.

The inductance L reached the maximum value of 0.41 H (larger than the design value, 0.28 H), under DC condition, then decreased as frequency increased. The current sweep rate of 4 A/s (Fig. 14) confirmed that the inductance L was 0.32 H according to equation $U = Ldi/dt$, Where U is the induced voltage of the magnet (about 1.28 V) and di/dt is 4 A/s. Compared to the 0.41 H tested by the LCR tester, 0.32 H is closer to the design value. The inductance changes and differences among the three values suggest that the metal structure of the conduction cooling produced an eddy current in the alternating magnetic field, and thus resulting in changes in inductance.

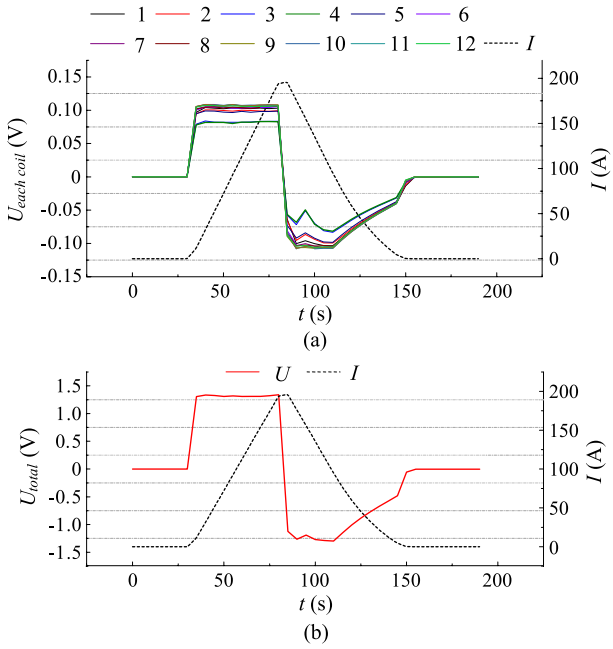

Fig. 14. Voltage variations of the magnet and coils during excitation. (a) Voltage variation of coils 1–12. (b) Voltage variation of the magnet.

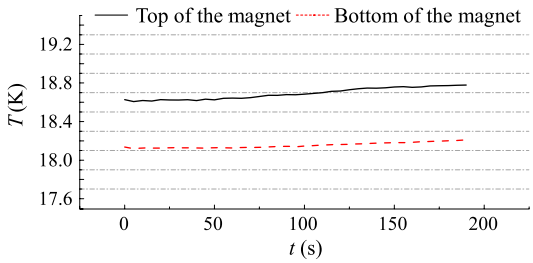

Fig. 15. Temperature of the magnet, where $I = 200$ A.

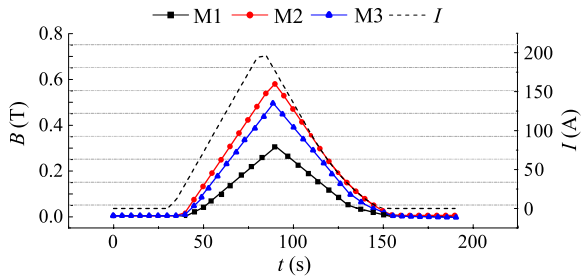

Fig. 16. Magnetic induction densities of the magnet, where $I = 200$ A.

C. Current-Carrying Characteristic

In order to demonstrate the prototype's current-carrying capability, the magnet was fed with the DC power supply and measured again as shown in Fig. 11. Current was fed at a sweep rate of 4 A/s to 200 A, held for 1 s, and then ramped down to zero with the same sweep rate. The voltage and temperature variations of magnet versus time are shown in Figs. 14 and 15, and the magnetic flux densities of M1, M2 and M3 versus time are depicted in Fig. 16.

When the current was kept at 200 A for 1 s, the resistance voltage of the magnet which was recorded by the quench protection system reached 139 mV (the inductive voltage was canceled). The resistance voltage of coil 8# was 16 mV, slightly higher than the quench transition voltage of 15 mV (under 1 μV/cm criterion, with tape length 150 m in each coil). The voltage values of other coils were lower than 10 mV.

The temperature variation range of the magnet was within 0.2 K. Considering the voltage of coil 8# was higher the quench transition voltage (15 mV), we considered 200 A as the maximal operating current of the magnet, which agrees with the design value—we should point out that the magnet system actually operated at a lower temperature (17.6 K) with respect to the design value (20 K) and this increases the current margin.

The magnetic flux densities of M1, M2 and M3 were about 0.3 T, 0.5 T and 0.6 T, respectively. We observed a time lag of about 10 s between the maximal current 200 A and the maximal magnetic flux densities. As shown in Fig. 9(c), the magnetic flux densities of M2 and M3 were between 0.4770 T and 0.5943 T, which is consistent with the measured values.

V. Conclusion

In this study, we designed and constructed a laboratory-scale YBCO toroidal magnet and performed a series of experiments to test its performance and validate our design. Some conclusions can be summarized as follows:

(1) The magnet can operate at 20 K when the excitation current is lower than 200 A. The maximal operating current is 200 A and the maximal energy storage is 6.4 kJ, so the prototype is able to satisfy the design requirements.

(2) When the magnet is in stable operation, the maximal temperature rise is within the range of 0.2 K.

(3) The magnetic flux densities between the two coils (M1) and inside the center of one of the coils (M2 or M3) are 0.3 T and 0.6 T, respectively, as consistent with the simulation results.

References

[1] Z. S. Hartwig, C. B. Haakonsen, R. T. Mumgaard, and L. Bromberg, "An initial study of demountable high-temperature superconducting toroidal field magnets for the Vulcan tokamak conceptual design," *Fusion Eng. Des.*, vol. 87, pp. 201–214, Nov. 2012.

[2] P. Komarek, "Potential and desire for HTS application in thermonuclear fusion," *Fusion Eng. Des.*, vol. 81, pp. 2287–2296, Sep. 2006.

[3] W. H. Fietz *et al.*, "Prospects of high temperature superconductors for fusion magnets and power applications," *Fusion Eng. Des.*, vol. 88, pp. 440–445, Mar. 2013.

[4] M. Gryaznevich *et al.*, "Progress in application of high temperature superconductor in tokamak magnets," *Fusion Eng. Des.*, vol. 88, pp. 1593–1596, Sep. 2013.

[5] R. M. Scanlan *et al.*, "Fabrication and test results for Rutherford-type cables made from BSCCO strands," *IEEE Trans. Appl. Supercond.*, vol. 9, no. 2, pp. 130–133, Jun. 1999.

[6] D. C. Van der Laan, H. J. N. Van Eck, B. Ten Haken, H. H. J. Ten Kate, and J. Schwartz, "Strain effects in high temperature superconductors investigated with magneto-optical imaging," *IEEE Trans. Appl. Supercond.*, vol. 13, no. 2, pp. 3534–3539, Jun. 2003.

[7] D. C. van der Laan *et al.*, "Effect of tensile strain on grain connectivity and flux pinning in $Bi_2Sr_2Ca_2Cu_3O_x$ tapes," *Appl. Phys. Lett.*, vol. 88, 2006, Art. no. 022511.

[8] L. Ren *et al.*, "The experimental research and analysis of a HTS SMES hybrid magnet," *IEEE Trans. Appl. Supercond.*, vol. 25, no. 3, Jun. 2015, Art. no. 5400205.

[9] J. File, R. G. Mills, and G. V. Sheffield, "Large superconducting magnet designs for fusion," *IEEE Trans. Nucl. Sci.*, vol. NS-18, no. 4, pp. 277–282, Jun. 1971.